Journal of Sound and Vibration (1998) **215**(1), 81–103
Article No. sv981615

A COMPARISON OF NEAR-FIELD ACOUSTIC ERROR SENSING STRATEGIES FOR THE ACTIVE CONTROL OF HARMONIC FREE FIELD SOUND RADIATION

X. Qiu, C. H. Hansen and X. Li

Department of Mechanical Engineering, *The University of Adelaide*, *South Australia* 5005, *Australia*

(*Received* 6 *August* 1997, *and in final form* 2 *March* 1998)

A theoretical comparison of a number of near-field acoustic error sensing strategies is undertaken for active control of harmonic free-field sound radiation. Error sensing strategies investigated include the minimization of acoustic potential energy density, acoustic kinetic energy density, total acoustic energy density and mean active sound intensity at a point and the minimization of the sum of each cost function at a number of points in the near field. The error sensing strategies are analyzed for harmonic sound fields radiated by a monopole primary source and a dipole-like pair of primary sources. The control source is a monopole radiating at the same frequency and the criterion used to assess the error sensing strategies is the minimization of the total radiated acoustic power. It was found that the most appropriate near-field acoustic error sensing strategy for the active control of harmonic free-field sound radiation is minimizing the sum of the weighted mean active intensity in the direction normal to the surface surrounding all the primary and control sources.

1. INTRODUCTION

Some of the first attempts to control sound radiation into free space can be found in the work directed at controlling tonal noise radiated by large electrical transformers [1–8]. From the first published attempt to control electrical transformer noise reported by Conover in 1956 to the more recently commercial "Quiet Power" system in the U.S. using small acoustic sources and piezoceramic patches to control transformer noise, a significant amount of research has been done on the active control of harmonic free-field sound radiation, but most of the research has focused upon control source design and location and the use of far-field error sensors. Research on acoustic control source can be loosely divided into two categories: control sources that are placed a relatively large distance from the primary source [9] (i.e., at a distance of the order of a wavelength or greater) and control sources that are placed close to the primary source [10, 11]. For each category, the control sources can be either arrays of monopoles or multipoles [12]. Research on error sensors has included the control of harmonic sound pressure at a point, the minimization of the sum of the squared pressure at a number of far-field error sensors and the minimization of the total acoustic power output [13–15].

The design of the "physical" part of the active noise control system involves several steps. One of the most important is to find the best locations of error sensors according to the primary source characteristics. Most of the work on optimizing the locations of the

0022–460X/98/310081 + 23 $30.00/0

acoustic error sensors has been focused on far-field sensors because usually far-field sound pressure level is the target to be controlled. Much of the previous work has also shown that minimizing the sound level at a number of error microphones at some distance from a transformer in the far acoustic field did not result in global noise reduction and also large variations in the sound pressure level occurred over time as a result of ground and atmospheric effects. In addition to the large variation with time of the sound level at the error sensors, atmospheric wind and temperature gradients cause sound waves to travel in curved paths and this often results in far-field error microphones not "sensing" sound that eventually finds its way into the community. Far-field error sensors also cause controller stability problems as a result of the large acoustic time delays which they introduce into the control system. Meanwhile, the optimum compactness of the whole system is not realized in practice when far-field error sensors are used. All of these problem can be solved by the use of near-field error sensors but the challenge is to find a convenient cost function to minimize which will result in the minimization of global radiated sound power. Until now, little work has been reported on the use of near-field acoustic error sensors for the active control of harmonic free-field sound radiation.

On the other hand, several near-field error sensing techniques involving structural vibration sensors have been developed for the minimization of structurally radiated sound [16–20]. Clark and Fuller have discussed the use of PVDF film modal sensors and feedforward control applied to rectangular acoustic radiators [16]. By choosing the appropriate location and shape of the PVDF film, only those structural modes that efficiently radiate to the far field are observed. Minimization of the amplitudes of these "radiation modes" is thus guaranteed to minimize the total sound power while eliminating the use of the far-field error microphones. Maillard and Fuller discussed advanced time domain wavenumber sensing for structural acoustic systems which implemented point structural sensors in parallel with an array of digital filters to obtain an error signal directly related to the far-field pressure in a prescribed direction [17]. The work has been extended by Tanaka, Snyder and Hansen to the active control of sound transmission into a coupled cavity by using distributed parameter modal sensors called "smart sensors" [18, 19]. More recently, Cazzolato and Hansen used finite element analysis to investigate the using of structural error sensors on more complex geometries [20].

Wang and Fuller presented a theoretical analysis of the near-field time averaged intensity and pressure distribution of actively controlled plate-radiated sound [21]. It was found that, although limited to the (3,1) mode resonance case, applying control leads to an overall fall in the magnitudes of the near-field pressure and intensity vectors while the complexity of the pressure field is markedly increased. They suggested that if a distributed pressure sensor was located near the plate, then minimizing the near-field sensor output might have the same control influences as far-field point sensors, at least for plate modes on resonance. But they did not prove that.

Active control of noise in ducts and enclosures has been widely investigated theoretically and experimentally with regard to various error sensor strategies: local sound pressure, total acoustic potential energy, downstream potential energy, positive-travelling pressure, total acoustic radiation power, acoustic radiation power of the control sources and the active sound intensity [22–24]. It was found generally that each strategy has been associated with a particular configuration and a particular objective for minimizing the sound field. A theoretical comparison of a number of error sensing strategies has also been undertaken [23] with the objective of determining an optimum strategy, appropriate for both plane wave and higher-order mode propagation for a range of duct termination conditions.

There may be two reasons for the small effort so far directed toward the use of near-field acoustic error sensors: one is that it is usually recognized that reductions in far-field pressure are often accompanied by increases in the near-field pressure [3, 13] and the other is the complex and extensive computations required for existing methods such as acoustic holography and the boundary element method [25–29]. The only work that the authors have found concerning the uses of near-field acoustic error sensors was presented by Hansen and Snyder [14] , who gave a figure illustrating the resultant power attenuation achieved by minimizing the acoustic pressure amplitude at a single location within a distance of one wavelength from the centre of monopole primary and control sources. They found that placing an error sensor in the near field of the primary source is a "risky" pursuit because the acoustic power attenuation achieved when minimizing the acoustic pressure at the sensor varied rapidly with the sensor location.

The objective of this paper is to extend the investigation of the minimization of near-field pressure at a point to the study of a number of different error sensing strategies such as the minimization of acoustic potential energy density, acoustic kinetic energy density, total acoustic energy density and mean active sound intensity at a point and the minimization of the sum of each cost function at a number of points in the near field. These error sensing strategies will be analyzed here for the harmonic sound field radiated by a monopole primary source and the harmonic field radiated by a dipole-like pair of primary sources. For both cases, the control source is a monopole radiating at the same frequency.

2. ACTIVE CONTROL OF HARMONIC FREE FIELD SOUND RADIATION

The sound pressure at some location $\mathbf{r}_e$ in space due to the harmonic operation of an acoustic monopole source located at a position $\mathbf{r}_q$ is

$$p(\mathbf{r}_e) = \frac{\mathrm{j}\omega\rho_0 q\ \mathrm{e}^{-\mathrm{j}kr}}{4\pi r}, \tag{1}$$

where $r = |\mathbf{r}_e - \mathbf{r}_q|$, q is the volume velocity of the monopole source, k is the acoustic wavenumber at the frequency ω of interest, ρ_0 is the mean air density and the positive harmonic time dependence of the form $\mathrm{e}^{\mathrm{j}\omega t}$ is implicit in the equation (this will be the case throughout the paper).

The particle velocity at location $\mathbf{r}_e$ only exists in the radial direction, and is defined as

$$\mathbf{u}(\mathbf{r}_e) = \frac{p(\mathbf{r}_e)}{\rho_0 c}\left(1 - \frac{\mathrm{j}\lambda}{2\pi r}\right)\frac{(\mathbf{r}_e - \mathbf{r}_q)}{r}, \tag{2}$$

where λ is the acoustic wavelength and c is the sound speed in air.

The fluid kinetic energy per unit volume is known as the "kinetic energy density", and at location $\mathbf{r}_e$ it is

$$T(\mathbf{r}_e) = \tfrac{1}{2}\rho_0|\mathbf{u}(\mathbf{r}_e)|^2. \tag{3}$$

The fluid potential energy per unit volume is known as the "potential energy density", and at location $\mathbf{r}_e$ it is

$$U(\mathbf{r}_e) = \frac{1}{2\rho_0 c^2}\,p(\mathbf{r}_e)^2. \tag{4}$$

The total mechanical energy per unit volume is known as the "sound energy density" or "total energy density", and at location $\mathbf{r}_e$ it is

$$E(\mathbf{r}_e) = T + U = \tfrac{1}{2}\rho_0|\mathbf{u}(\mathbf{r}_e)|^2 + \frac{1}{2\rho_0 c^2}\,p(\mathbf{r}_e)^2. \tag{5}$$

The expression for the mean active intensity directed from $\mathbf{r}_p$ to $\mathbf{r}_e$ at location $\mathbf{r}_e$ is [30, 31]

$$\mathbf{I}(\mathbf{r}_e) = \tfrac{1}{2}\,\mathrm{Re}\,\{p(\mathbf{r}_e)\mathbf{u}^*(\mathbf{r}_e)\}. \tag{6}$$

As the system being considered is linear, the concept of superposition is valid, so that the total sound pressure and particle velocity at location $\mathbf{r}_e$, radiated from a monopole primary source and a monopole control source or that radiated by an acoustic dipole-like pair of monopole primary sources with a monopole control source, can be obtained by simple superposition (vectors superposition for velocity). Then the total kinetic energy, the total potential energy, the total mechanical energy and the total mean active intensity can be easily deduced through equations (3) to (6).

The value of the function F, to be minimized under the influence of the primary and control sources can be expressed as a quadratic function of the control source volume velocity $\mathbf{Q}_c = [q_{c,1}\ \ q_{c,2}\ \cdots\ q_{c,Nc}]^T$, for N_c control sources, such that [13]

$$F = \mathbf{Q}_c^H\mathbf{a}\mathbf{Q}_c + \mathbf{b}_1\mathbf{Q}_c + \mathbf{Q}_c^H\mathbf{b}_2 + c_p, \tag{7}$$

the composition of the matrices $\mathbf{a}$, $\mathbf{b}_1$, $\mathbf{b}_2$ and the value of the variable c_p are all dependent upon F, and their specific form will be outlined for each error sensor strategy. The matrix form of the proceeding equation allows any number of primary and control sources. Differentiating equation (7) with respect to the control sources volume velocity vector $\mathbf{Q}_c$, and equating the result to zero, yields the optimum control source volume velocity as

$$\mathbf{Q}_{copt} = -\tfrac{1}{2}\mathbf{a}^{-1}(\mathbf{b}_1^H + \mathbf{b}_2). \tag{8}$$

3. ERROR SENSING STRATEGIES

The criteria which are considered in the paper are the minimization of: (1) the potential energy density at a point (this is equivalent to the minimization of the sound pressure at a point); (2) the kinetic energy density at a point (this is equivalent to the minimization of the squared particle velocity at a point); (3) the total energy density at a point; (4) the mean active intensity in the radial direction at a point; (5) the sum of the potential energy density at a number of points through the near field (this is equivalent to the minimization of the sum of the squared pressure at a number of points throughout the near field); (6) the sum of the kinetic energy density at a number of points through the near field (this is equivalent to the minimization of the sum of the squared particle velocity at a number of points throughout the near field); (7) the sum of the total energy density at a number of points through the near field; (8) the sum of the mean active intensity in the radial direction at a number of points encompassing the sound sources.

It is assumed the acoustic centre of the primary and control sources is at the origin of the spherical co-ordinate system, so the total radiated acoustic power is equal to the integration of the mean acoustic intensity out of the sphere encompassing the sound sources. The sum of the mean active intensity in the radial direction at a number of near-field points encompassing the sound sources is an approximation of the total acoustic power; therefore the mean active intensity in the radial direction is selected as the minimized objective.

Minimization of the total acoustic power output of the primary and control sources is difficult in a practical context, and hence is treated chiefly as a theoretical strategy and as a criterion used to assess other error sensor strategies in this paper. The minimized total radiated acoustic power (obtained by far-field intensity integration or near-field analysis) when the total power output is selected as the criterion to be minimized is [14],

$$W_{min} = \frac{\omega^2 \rho_0}{8\pi c} |q_p|^2 (1 - \mathrm{sinc}^2 kd), \tag{9}$$

for the single monopole primary source/single monopole control source system. d is the distance between the primary and control sources and q_p is the primary source volume velocity.

The minimum total radiated acoustic power for a dipole-like pair of primary sources/single monopole control source system when the total power output is selected as criterion is [14],

$$W_{min} = \frac{\omega^2 \rho_0}{8\pi c} |q_p|^2 \{2[1 - \mathrm{sinc}(kd_p)] - [\mathrm{sinc}(kd_1) - \mathrm{sinc}(kd_2)]^2\}, \tag{10}$$

where q_p is the primary source volume velocity, taken to be equal in amplitude but opposite in sign for two primary monopole sources, d_1 and d_2 are the separation distances between the control source and two primary sources, and d_p is the separation distance between the two primary sources.

Assuming there are N_p primary sources with the volume velocity $\mathbf{Q}_p = [q_{p,1} \;\; q_{p,2} \;\; \cdots \;\; q_{p,Np}]^T$, for the error criterion of minimization of the sum of the potential energy density at N_e points through the near field, the error function F and matrices in equation (7) take the form

$$F = \sum_{i=1}^{N_e} U(\mathbf{r}_i), \tag{11}$$

$$\mathbf{a} = \frac{1}{2\rho_0 c^2} \mathbf{Z}_c^H \mathbf{Z}_c, \tag{12}$$

$$\mathbf{b}_1 = \frac{1}{2\rho_0 c^2} \mathbf{Q}_p^H \mathbf{Z}_p^H \mathbf{Z}_c, \tag{13}$$

$$\mathbf{b}_2 = \frac{1}{2\rho_0 c^2} \mathbf{Z}_c^H \mathbf{Z}_p \mathbf{Q}_p, \tag{14}$$

$$c_p = \frac{1}{2\rho_0 c^2} \mathbf{Q}_p^H \mathbf{Z}_p^H \mathbf{Z}_p \mathbf{Q}_p, \tag{15}$$

where $\mathbf{Z}_p$, an $N_e \times N_p$ matrix and $\mathbf{Z}_c$, an $N_e \times N_c$ matrix are the matrices of the transfer functions between the pressure at N_e error locations and N_p primary and N_c control source volume velocities respectively:

$$\mathbf{Z}_p = \begin{bmatrix} \mathbf{z}_p(\mathbf{r}_1)^T \\ \mathbf{z}_p(\mathbf{r}_2)^T \\ \vdots \\ \mathbf{z}_p(\mathbf{r}_{N_e})^T \end{bmatrix}, \qquad \mathbf{Z}_c = \begin{bmatrix} \mathbf{z}_c(\mathbf{r}_1)^T \\ \mathbf{z}_c(\mathbf{r}_2)^T \\ \vdots \\ \mathbf{z}_c(\mathbf{r}_{N_e})^T \end{bmatrix}. \tag{16}$$

$\mathbf{z}_p(\mathbf{r}_i)$ is the $N_p \times 1$ vector of the transfer functions between the pressure at the error location $\mathbf{r}_i$ and the primary source volume velocity, and $\mathbf{z}_c(\mathbf{r}_i)$ is the $N_c \times 1$ vector of the

transfer function between the pressure at the error location $\mathbf{r}_i$ and the control source volume velocity,

$$\mathbf{z}_p(\mathbf{r}_i) = \begin{bmatrix} z_{p,1}(\mathbf{r}_i) \\ z_{p,2}(\mathbf{r}_i) \\ \vdots \\ z_{p,N_p}(\mathbf{r}_i) \end{bmatrix}, \qquad \mathbf{z}_c(\mathbf{r}_i) = \begin{bmatrix} z_{c,1}(\mathbf{r}_i) \\ z_{c,2}(\mathbf{r}_i) \\ \vdots \\ z_{c,N_c}(\mathbf{r}_i) \end{bmatrix}, \tag{17}$$

where $z_{p,m}(\mathbf{r}_i)$ and $z_{c,n}(\mathbf{r}_i)$, the transfer function between the pressure at the error location $\mathbf{r}_i$ and the volume velocity of the mth primary source located at $\mathbf{r}_{p,m}$ and nth control source located at $\mathbf{r}_{c,n}$, can be obtained from equation (1),

$$z_{p,m}(\mathbf{r}_i) = \frac{\mathrm{j}\omega\rho_0 \, \mathrm{e}^{-\mathrm{j}k|\mathbf{r}_i - \mathbf{r}_{p,m}|}}{4\pi|\mathbf{r}_i - \mathbf{r}_{p,m}|}, \qquad z_{c,n}(\mathbf{r}_i) = \frac{\mathrm{j}\omega\rho_0 \, \mathrm{e}^{-\mathrm{j}k|\mathbf{r}_i - \mathbf{r}_{c,n}|}}{4\pi|\mathbf{r}_i - \mathbf{r}_{c,n}|}. \tag{18}$$

The minimization of the potential energy density at a point is a subset of this strategy for the case of $N_e = 1$.

For the error criterion of minimization of the sum of the kinetic energy density at N_e points through the near field, the error function F and matrices in equation (7) take the form

$$F = \sum_{i=1}^{N_e} T(\mathbf{r}_i), \tag{19}$$

$$\mathbf{a} = \tfrac{1}{2}\rho_0 \mathbf{Y}_c^H \mathbf{Y}_c, \tag{20}$$

$$\mathbf{b}_1 = \tfrac{1}{2}\rho_0 \mathbf{Q}_p^H \mathbf{Y}_p^H \mathbf{Y}_c, \tag{21}$$

$$\mathbf{b}_2 = \tfrac{1}{2}\rho_0 \mathbf{Y}_c^H \mathbf{Y}_p \mathbf{Q}_p, \tag{22}$$

$$c_p = \tfrac{1}{2}\rho_0 \mathbf{Q}_p^H \mathbf{Y}_p^H \mathbf{Y}_p \mathbf{Q}_p, \tag{23}$$

where $\mathbf{Y}_p$, an $N_e \times N_p$ matrix and $\mathbf{Y}_c$, an $N_e \times N_c$ matrix are the matrices of the transfer functions between the particle velocity at N_e error locations and N_p primary and N_c control source volume velocities respectively:

$$\mathbf{Y}_p = \begin{bmatrix} \mathbf{y}_p(\mathbf{r}_1)^T \\ \mathbf{y}_p(\mathbf{r}_2)^T \\ \vdots \\ \mathbf{y}_p(\mathbf{r}_{N_e})^T \end{bmatrix}, \qquad \mathbf{Y}_c = \begin{bmatrix} \mathbf{y}_c(\mathbf{r}_1)^T \\ \mathbf{y}_c(\mathbf{r}_2)^T \\ \vdots \\ \mathbf{y}_c(\mathbf{r}_{N_e})^T \end{bmatrix}, \tag{24}$$

$\mathbf{y}_p(\mathbf{r}_i)$ is the $N_p \times 1$ vector of the transfer function between the particle velocity at the error location $\mathbf{r}_i$ and the primary source volume velocity, and $\mathbf{y}_c(\mathbf{r}_i)$ is the $N_c \times 1$ vector of the transfer function between the pressure at the error location $\mathbf{r}_i$ and the control source volume velocities,

$$\mathbf{y}_p(\mathbf{r}_i) = \begin{bmatrix} \mathbf{y}_{p,1}(\mathbf{r}_i) \\ \mathbf{y}_{p,2}(\mathbf{r}_i) \\ \vdots \\ \mathbf{y}_{p,N_p}(\mathbf{r}_i) \end{bmatrix}, \qquad \mathbf{y}_c(\mathbf{r}_i) = \begin{bmatrix} \mathbf{y}_{c,1}(\mathbf{r}_i) \\ \mathbf{y}_{c,2}(\mathbf{r}_i) \\ \vdots \\ \mathbf{y}_{c,N_c}(\mathbf{r}_i) \end{bmatrix}, \tag{25}$$

where $\mathbf{y}_{p,m}(\mathbf{r}_i)$ and $\mathbf{y}_{c,n}(\mathbf{r}_i)$, are the transfer functions between the particle velocity at the error location $\mathbf{r}_i$ and the volume velocity of respectively the mth primary source located at $\mathbf{r}_{p,m}$ and the nth control source located at $\mathbf{r}_{c,n}$, and can be obtained from equation (2),

$$\mathbf{y}_{p,m}(\mathbf{r}_i) = \frac{z_{p,m}(\mathbf{r}_i)}{\rho_0 c}\left(1 - \frac{\mathrm{j}\lambda}{2\pi|\mathbf{r}_i - \mathbf{r}_{p,m}|}\right)\frac{(\mathbf{r}_i - \mathbf{r}_{p,m})}{|\mathbf{r}_i - \mathbf{r}_{p,m}|},$$

$$\mathbf{y}_{c,n}(\mathbf{r}_i) = \frac{z_{c,n}(\mathbf{r}_i)}{\rho_0 c}\left(1 - \frac{\mathrm{j}\lambda}{2\pi|\mathbf{r}_i - \mathbf{r}_{c,n}|}\right)\frac{(\mathbf{r}_i - \mathbf{r}_{c,n})}{|\mathbf{r}_i - \mathbf{r}_{c,n}|}. \tag{26}$$

In the preceding calculations, the vectors are decomposed into rectangular co-ordinates so that they can be calculated easily. The minimization of the kinetic energy density at a point is a subset of this strategy for the case of $N_e = 1$.

For the error criterion of minimization of the sum of the total energy density at N_e points through the near field, the error function F and matrices in equation (7) take the form

$$F = \sum_{i=1}^{N_e} E(\mathbf{r}_i) = \sum_{i=1}^{N_e} [T(\mathbf{r}_i) + U(\mathbf{r}_i)], \tag{27}$$

$$\mathbf{a} = \tfrac{1}{2}\rho_0 \mathbf{Y}_c^H \mathbf{Y}_c + \frac{1}{2\rho_0 c^2}\mathbf{Z}_c^H \mathbf{Z}_c, \tag{28}$$

$$\mathbf{b}_1 = \tfrac{1}{2}\rho_0 \mathbf{Q}_p^H \mathbf{Y}_p^H \mathbf{Y}_c + \frac{1}{2\rho_0 c^2}\mathbf{Q}_p^H \mathbf{Z}_p^H \mathbf{Z}_c, \tag{29}$$

$$\mathbf{b}_2 = \tfrac{1}{2}\rho_0 \mathbf{Y}_c^H \mathbf{Y}_p \mathbf{Q}_p + \frac{1}{2\rho_0 c^2}\mathbf{Z}_c^H \mathbf{Z}_p \mathbf{Q}_p, \tag{30}$$

$$c_p = \tfrac{1}{2}\rho_0 \mathbf{Q}_p^H \mathbf{Y}_p^H \mathbf{Q}_p \mathbf{Y}_p + \frac{1}{2\rho_0 c^2}\mathbf{Q}_p^H \mathbf{Z}_p^H \mathbf{Z}_p \mathbf{Q}_p, \tag{31}$$

where $\mathbf{Y}_p$, $\mathbf{Y}_c$, $\mathbf{Z}_p$, $\mathbf{Z}_c$ and $\mathbf{Q}_p$ are defined using the above equations to minimize the sum of the potential and kinetic energies. The minimization of the total energy density at a point is a subset of this strategy for the case of $N_e = 1$.

For the error criterion of minimization of the sum of the mean active intensity in the radial direction at N_e points through the near field using one monopole control source, the error function F and matrices in equation (7) take the form

$$F = \sum_{i=1}^{N_e} \mathbf{I}(\mathbf{r}_i) = \tfrac{1}{2}\sum_{i=1}^{N_e} \mathrm{Re}\,\{\mathbf{u}^*(\mathbf{r}_i)p(\mathbf{r}_i)\}, \tag{32}$$

$$\mathbf{a} = \tfrac{1}{2}\frac{\mathbf{Y}_c^H \mathbf{Z}_c + \mathbf{Y}_c^T \mathbf{Z}_c^*}{2} = \tfrac{1}{2}\mathrm{Re}\,\{\mathbf{Y}_c^H \mathbf{Z}_c\}, \tag{33}$$

$$\mathbf{b}_1 = \tfrac{1}{2}\frac{\mathbf{Q}_p^H \mathbf{Y}_p^H \mathbf{Z}_c + \mathbf{Y}_c^T \mathbf{Z}_p^* \mathbf{Q}_p^*}{2} \tag{34}$$

$$\mathbf{b}_2 = \tfrac{1}{2}\frac{\mathbf{Y}_c^H \mathbf{Z}_p \mathbf{Q}_p + \mathbf{Q}_p^T \mathbf{Y}_p^T \mathbf{Z}_c^*}{2}, \tag{35}$$

$$c_p = \tfrac{1}{2}\mathrm{Re}\,\{\mathbf{Q}_p^H \mathbf{Y}_p^H \mathbf{Z}_p \mathbf{Q}_p\}, \tag{36}$$

where equations (33)–(35) are obtained using

$$\mathbf{Q}_c^H = \mathbf{Q}_c^*, \qquad \mathbf{Q}_c = \mathbf{Q}_c^T. \tag{37}$$

In the calculation, $\mathbf{Y}_p$, $\mathbf{Y}_c$, $\mathbf{Z}_p$, $\mathbf{Z}_c$ and $\mathbf{Q}_p$ are defined as above except that $y_{p,m}(\mathbf{r}_i)$ and $y_{c,n}(\mathbf{r}_i)$ are changed to denote the transfer function between the particle velocity in the radial direction at the error location $\mathbf{r}_i$, and the volume velocity of the mth primary source located at $\mathbf{r}_{p,m}$, and the control source located at $\mathbf{r}_{c,1}$ respectively, in the form of scalars,

$$y_{p,m}(\mathbf{r}_i) = \frac{z_{p,m}(\mathbf{r}_i)}{\rho_0 c}\left(1 - \frac{\mathrm{j}\lambda}{2\pi|\mathbf{r}_i - \mathbf{r}_{p,m}|}\right)\frac{(\mathbf{r}_i - \mathbf{r}_{p,m})}{|\mathbf{r}_i - \mathbf{r}_{p,m}|}\cdot\frac{\mathbf{r}_i}{|\mathbf{r}_i|},$$

$$y_{c,1}(\mathbf{r}_i) = \frac{z_{c,1}(\mathbf{r}_i)}{\rho_0 c}\left(1 - \frac{\mathrm{j}\lambda}{2\pi|\mathbf{r}_i - \mathbf{r}_{c,1}|}\right)\frac{(\mathbf{r}_i - \mathbf{r}_{c,1})}{|\mathbf{r}_i - \mathbf{r}_{c,1}|}\cdot\frac{\mathbf{r}_i}{|\mathbf{r}_i|}. \tag{38}$$

It should be noted a unique minimum only exists when $\mathbf{a}$ is positive. This can be easily proved as follows:

$$\begin{aligned}
\mathbf{a} &= \mathbf{a}(1,1)\\
&= \tfrac{1}{2}\sum_{i=1}^{N_e} \mathrm{Re}\,\{y_{c,1}^*(\mathbf{r}_i) z_{c,1}(\mathbf{r}_i)\}\\
&= \tfrac{1}{2}\sum_{i=1}^{N_e} \mathrm{Re}\left\{\left(1 + \frac{\mathrm{j}\lambda}{2\pi|\mathbf{r}_i - \mathbf{r}_{c,1}|}\right)\frac{(\mathbf{r}_i - \mathbf{r}_{c,1})}{|\mathbf{r}_i - \mathbf{r}_{c,1}|}\cdot\frac{\mathbf{r}_i}{|\mathbf{r}_i|} z_{c,1}^*(\mathbf{r}_i) z_{c,1}(\mathbf{r}_i)\right\}\\
&= \tfrac{1}{2}\sum_{i=1}^{N_e} \frac{(\mathbf{r}_i - \mathbf{r}_{c,1})}{|\mathbf{r}_i - \mathbf{r}_{c,1}|}\cdot\frac{\mathbf{r}_i}{|\mathbf{r}_i|}\left[\frac{\omega\rho_0}{4\pi|\mathbf{r}_i - \mathbf{r}_{c,1}|}\right]^2
\end{aligned} \tag{39}$$

and

$$\frac{(\mathbf{r}_i - \mathbf{r}_{c,1})}{|\mathbf{r}_i - \mathbf{r}_{c,1}|}\cdot\frac{\mathbf{r}_i}{|\mathbf{r}_i|} > \mathbf{0} \qquad \text{if} \qquad |\mathbf{r}_i - \mathbf{r}_{c,1}|^2 + |\mathbf{r}_i|^2 > |\mathbf{r}_{c,1}|^2. \tag{40}$$

If equation (40) is satisfied, then a unique minimum can be guaranteed. The minimization of the mean active intensity in the radial direction at a point is a subset of this strategy for the case of $N_e = 1$.

4. RESULTS

For the results presented here, a black box ideal feedforward controller has been assumed. The design of a feedforward active control system can be viewed as a hierarchical procedure aimed at optimizing the performance of the four principal components of the system; introduction of the control signal, extraction of an error signal, acquisition of a primary disturbance-correlated reference signal for the controller and design of the controller itself. If any one of the stages is improperly designed then the system is doomed, as it is only as good as its weakest link. For the systems considered in this paper, the location of the control monopole is typical [14], the error signal is obtained via the strategies outlined in the previous section and fed to the controller, the reference signal is obtained from the input to the primary source while the controller is assumed to be ideal.

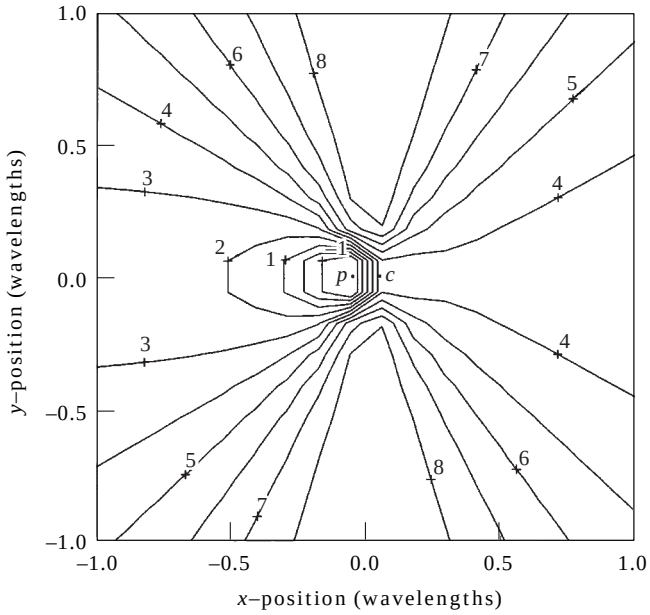

Figure 1. Maximum achievable acoustic power attenuation (dB) as a function of error sensor location for the minimization of potential energy density at a point. Single monopole primary and control sources separated by $\lambda/10$.

The first arrangement considered here is the most simple system of all, where a single monopole control source located at $(\lambda/20,0)$ is used to attenuate the acoustic radiation from a single monopole primary source located at $(-\lambda/20,0)$ in 2-D rectangular co-ordinates. The distance between them is $\lambda/10$, which places an absolute bound upon

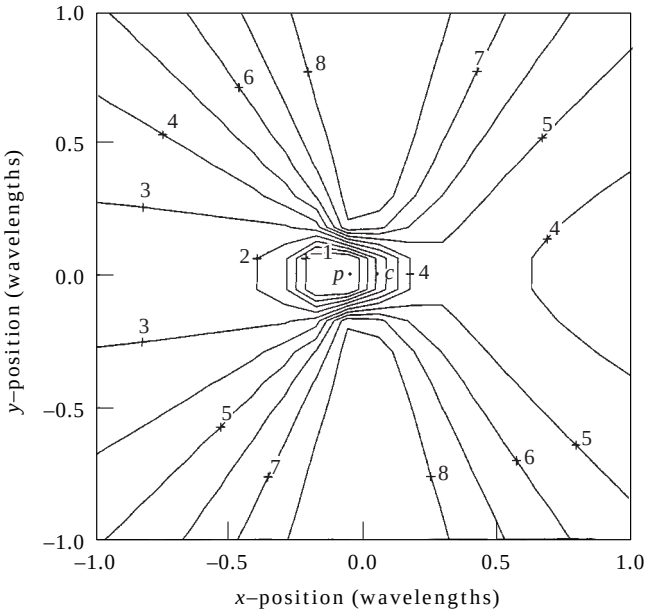

Figure 2. Maximum achievable acoustic power attenuation (dB) as a function of error sensor location for the minimization of kinetic energy density at a point. Single monopole primary and control sources separated by $\lambda/10$.

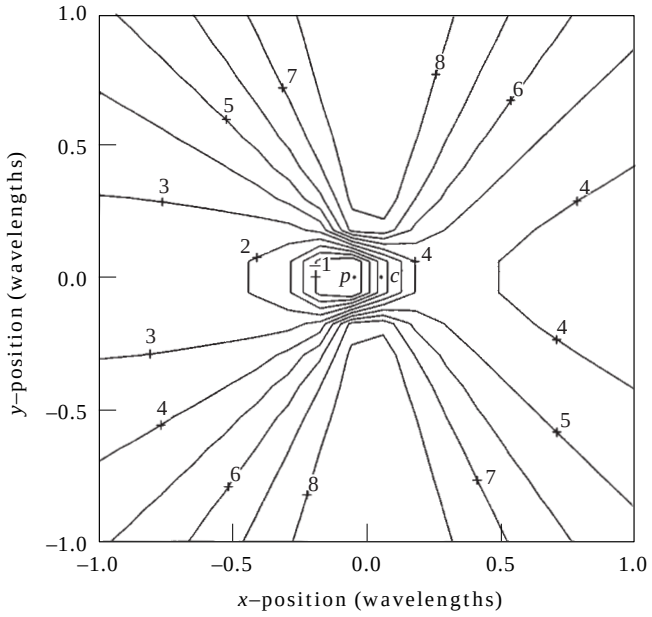

Figure 3. Maximum achievable acoustic power attenuation (dB) as a function of error sensor location for the minimization of total energy density at a point. Single monopole primary and control sources separated by $\lambda/10$.

the level of acoustic power attenuation of 9·0 dB. The acoustic power attenuation is defined here as $10 \log_{10} (W_{unc}/W_{cont})$. W_{unc} is the acoustic power of the primary source while W_{cont} is the total acoustic power of the whole system including the primary source and optimum control source.

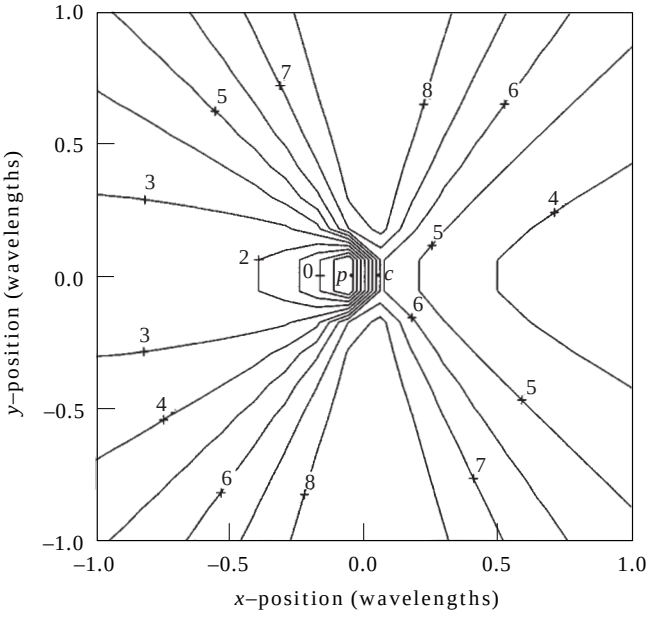

Figure 4. Maximum achievable acoustic power attenuation (dB) as a function of error sensor location for the minimization of mean active intensity in the radial direction at a point. Single monopole primary and control sources separated by $\lambda/10$.

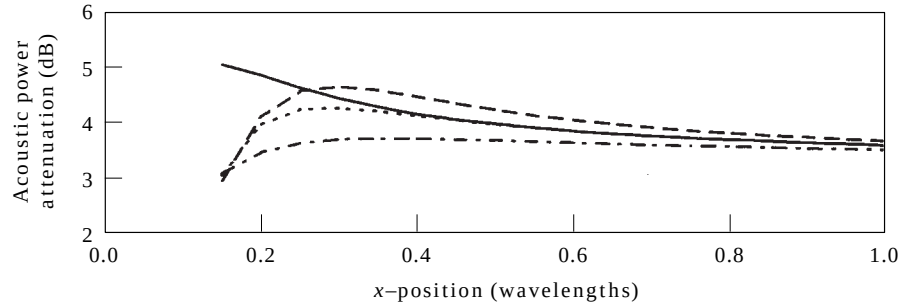

Figure 5. Maximum achievable acoustic power attenuation as a function of error sensor location on the control source side of the control source/primary source axis for the minimization of all four criteria: ·– ·– ·–, potential; ------, kinetic; · · · · · · · · · , total energy; ——, intensity. Single monopole primary and control sources separated by $\lambda/10$.

Figures 1 to 4 illustrate the resultant power attenuation from minimizing the first four criteria respectively at a single location in the near field (within a distance of one wavelength from the centre of the primary and control sources) for harmonic excitation. The first four criteria are the minimization of the potential energy density at a point, the kinetic energy density at a point, the total energy density at a point and the mean active intensity in the radial direction at a point. Note that Figure 1 is after Hansen and Snyder [14], which is included in this paper for comparison.

From the acoustic power attenuation contours in Figures 1–4, it is readily apparent that at about one wavelength distance from the centre of the primary and control sources the four criteria are nearly the same. However, when the error sensor approaches the mid-point between the two sources, the acoustic power attenuation achieved by the four criteria becomes different. This is in agreement with theory [31] because the far field (at a distance of the order of one wavelength or greater) is characterized by simple relationships valid for a plane wave; to the first order in $1/kr$, $u_r \rightarrow p/\rho_0 c$ and $u_\theta \rightarrow 0$ and $u_\varphi \rightarrow 0$; to the second order, $E \rightarrow |p|^2/\rho_0 c^2 = \rho_0 |u_r|^2$ and $I_r = Ec$. Therefore, in the far field all the four criteria are the same.

Although at the same point in the near field, the acoustic power attenuation achieved by different criteria have different values; for example, at the point ($\lambda/8$, 0) the achieved acoustic power attenuation is 2·72 dB, 2·13 dB, 2·27 dB and 5·00 dB for potential, kinetic, total energy density and sound intensity, respectively, and each criterion has its own optimum point; yet if one region (not very near the sources) is good for one criterion, it is usually also a good error sensor location for the others. This can be observed in Figures 1–4 where the contours in each figure have similar shapes. The nearest optimum error sensor placements for all four criteria will fall on a line perpendicular to the control source/primary source axis, centred at a position between the primary and control sources and always closer to the control sources. The worst error sensor placements are those approaching the primary source from the primary source side.

The differences in the four criteria can be more clearly illustrated in Figure 5. As the error sensors approach the mid-point between two sources, when the distance is larger than about $\lambda/4$, the kinetic energy density strategy is the best and the potential energy density strategy is the worst, while when the error sensor is quite near the mid-point between two sources (within $\lambda/4$), the intensity strategy becomes the best, the kinetic energy density strategy becomes the worst and the total energy density strategy is between the two.

Figures 6–9 show the results of minimizing the sum of each cost function over a number of sensor locations. The sensors are located evenly on a circle surrounding the primary

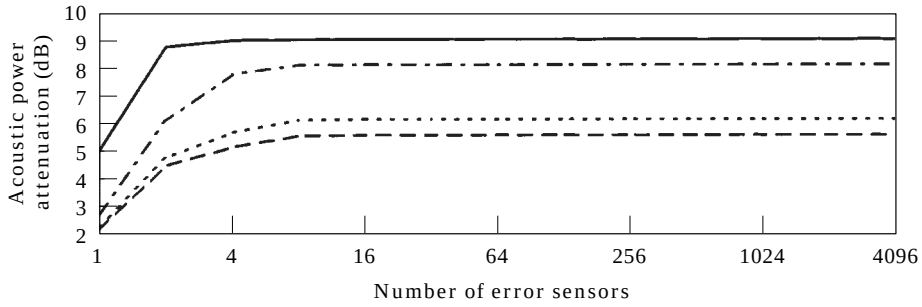

Figure 6. Sound power attenuation as a function of error sensor number for minimization of the sum of each cost function: ·– ·– ·–, potential; ------, kinetic; · · · · · · · · · , total energy; ——, intensity. The sensors are located evenly on the circle with a radius of $\lambda/8$ centred at the acoustic centre of the primary and control sources. Single monopole primary and control sources separated by $\lambda/10$.

and control sources with different radii in the xy plane. The first error sensor location is at the (+radius, 0), then including location (−radius, 0), and then (0, radius) and (0, −radius) … etc. The solid lines represent the results from minimizing the sum of the mean active sound intensity in the radial direction, the dashed lines represent the results from minimizing the sum of the kinetic energy density, the dotted lines represent that for the total energy density and the dash–dot lines are for the potential energy density. Note that the four lines are coincident in Figure 9 because they have the same value.

There are two important points which are evident from the results. First, close to optimal results can be achieved with a relatively small number of sensors (eight, for example) in the far field or near field (not quite near the centre, but beyond $\lambda/4$) by adjusting the control source strength to minimize the sum of any cost function. The results from early research undertaken by Nelson and Elliott [13] gave the same conclusion for minimizing the sum of the squared pressure at several angular locations in the far field. Second, when the error sensors are quite close to the sources (within $\lambda/8$), the acoustic power attenuation achieved by minimizing the sum of each cost function are different; the best results are obtained by minimizing the sum of the mean active sound intensity in the radial direction, and the worst is from the kinetic energy density minimization.

The next arrangement to be considered is that of a single monopole control source located at ($\lambda/6$, 0) being used to attenuate acoustic radiation from a dipole-like pair of

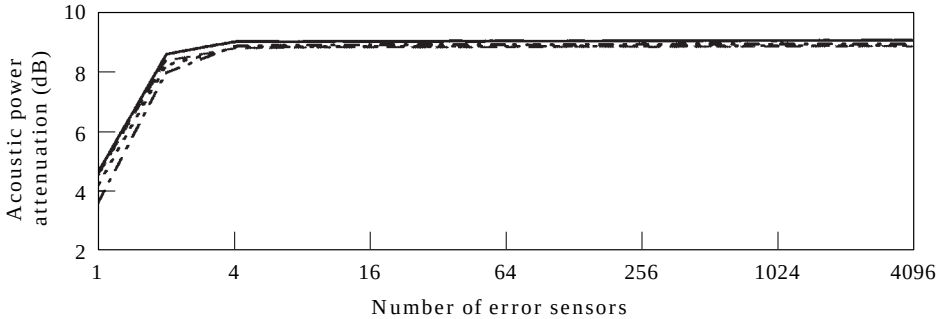

Figure 7. Sound power attenuation as a function of error sensor number for minimization of the sum of each cost function: ·– ·– ·–, potential; ------, kinetic; · · · · · · · · · , total energy; ——, intensity. The sensors are located evenly on the circle with a radius of $\lambda/4$ centred at the acoustic centre of the primary and control sources. Single monopole primary and control sources separated by $\lambda/10$.

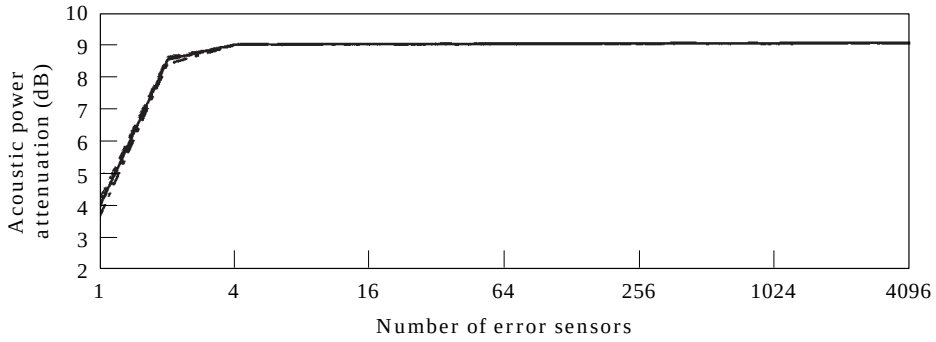

Figure 8. Sound power attenuation as a function of error sensor number for minimization of the sum of each cost function: ·– ·– ·–, potential; ------, kinetic; · · · · · · · · · , total energy; ——, intensity. The sensors are located evenly on the circle with a radius of $\lambda/2$ centred at the acoustic centre of the primary and control sources. Single monopole primary and control sources separated by $\lambda/10$.

primary sources located at $(-\lambda/6 - \lambda/20,\ 0)$ and $(-\lambda/6 + \lambda/20,\ 0)$ in rectangular co-ordinates. Note that the control source is at one of the optimum locations, which place an absolute bound upon the level of acoustic power attenuation of 3·7 dB. Details about the arrangement can be found in reference [14].

Figures 10–13 illustrate the resultant power attenuation achieved by minimizing the first four criteria respectively at a single location in the near field (within a distance of one wavelength from the centre of the primary and control sources) for harmonic excitation. Figure 14 shows the acoustic power attenuation as a function of error sensor location along the control source side of the control source/primary source axis for the minimization of all four criteria. Figures 15–18 show the results achieved by minimizing the sum of each cost function over a number of error sensor locations. The sensors are located evenly on a circle surrounding the primary and control sources with different radii in the xy plane. The first error sensor location is at the (+radius, 0), then (−radius, 0), and then (0, radius) and (0, −radius) …etc. Note that the four lines are coincident in Figure 18 because they have the same value.

After examining Figures 10–18, it can be seen that the following results also characterize the dipole-like pair of primary sources/single monopole control source system: all the eight criteria give the same results in the far field; if one region in the near field (not very near

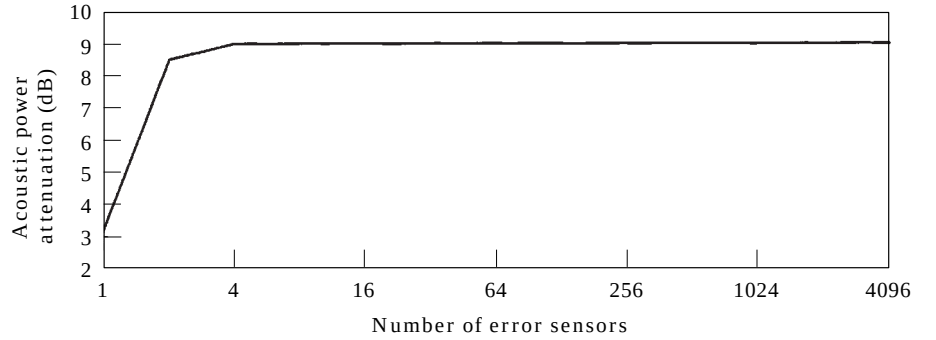

Figure 9. Sound power attenuation as a function of error sensor number for minimization of the sum of each cost function: ·– ·– ·–, potential; ------, kinetic; · · · · · · · · · , total energy; ——, intensity. The sensors are located evenly on the circle with a radius of 100λ centred at the acoustic centre of the primary and control sources. Single monopole primary and control sources separated by $\lambda/10$.

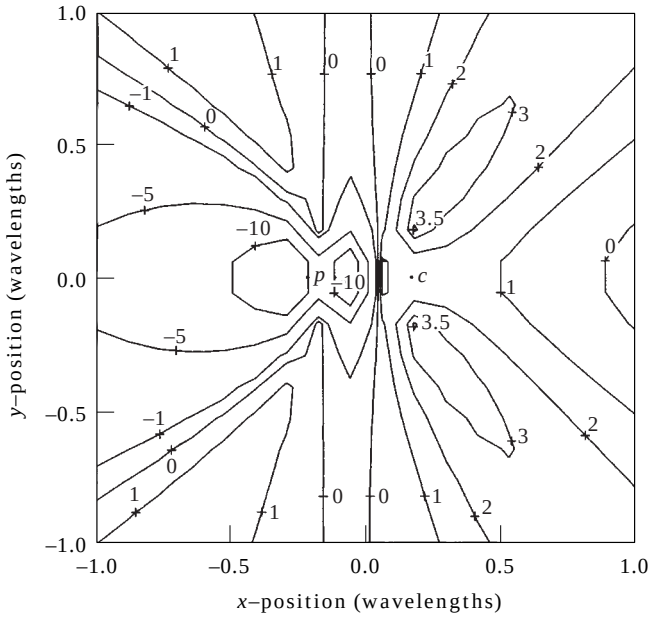

Figure 10. Maximum achievable acoustic power attenuation (dB) as a function of error sensor location for the minimization of potential energy density at a point. Dipole-like pair of primary sources and a single monopole control source separated by $\lambda/3$.

the sources) is good for one criterion, it is usually also a good error sensor location region for the others and *vice versa*; the worst error sensor placements are those approaching the primary source from the primary source side; there are differences among different criteria, especially when the error sensors approach the mid-point between primary and control

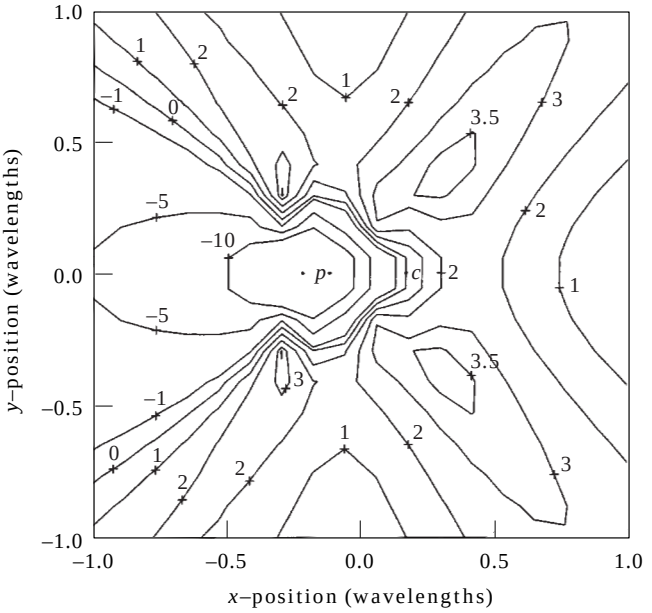

Figure 11. Maximum achievable acoustic power attenuation (dB) as a function of error sensor location for the minimization of kinetic energy density at a point. Dipole-like pair of primary sources and a single monopole control source separated by $\lambda/3$.

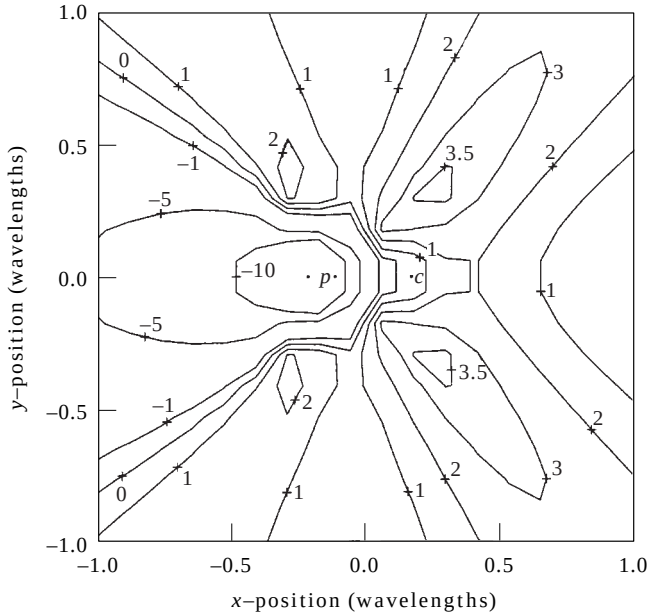

Figure 12. Maximum achievable acoustic power attenuation (dB) as a function of error sensor of total energy density at a point. Dipole-like pair of primary sources and a single monopole control source separated by $\lambda/3$.

sources. When the error sensor is quite near the mid-point between primary and control sources (within $\lambda/4$), the intensity strategy becomes the best and the kinetic energy density strategy becomes the worst; close to optimal results can be achieved with a relatively small number of sensors in the far field or near field (not quite near) by adjusting the control

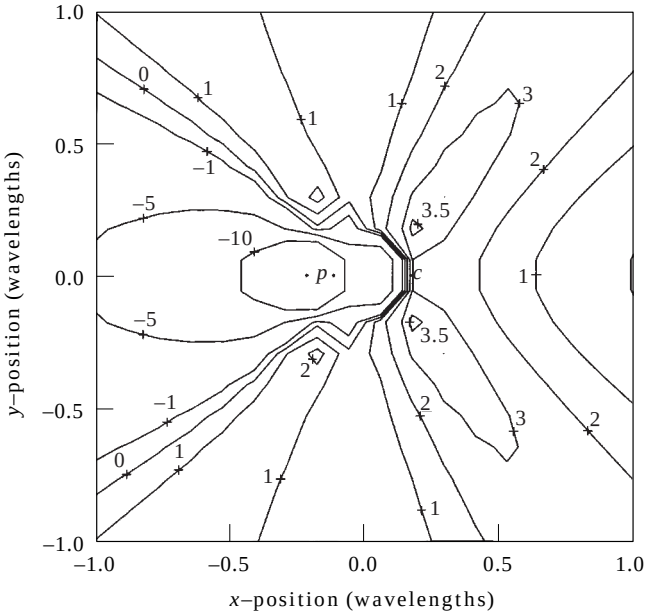

Figure 13. Maximum achievable acoustic power attenuation (dB) as a function of error sensor location for the minimization of mean active intensity in the radial direction at a point. Dipole-like pair of primary sources and a single monopole control source separated by $\lambda/3$.

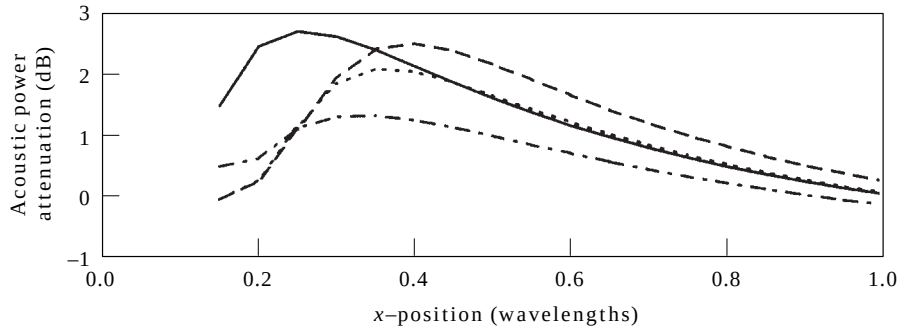

Figure 14. Maximum achievable acoustic power attenuation as a function of error sensor location on the control source side of the control source/primary source axis for the minimization of all four criteria: ·– ·– ·–, potential; ------, kinetic; · · · · · · · · · , total energy; ——, intensity. Dipole-like pair of primary sources and a single monopole control source separated by $\lambda/3$.

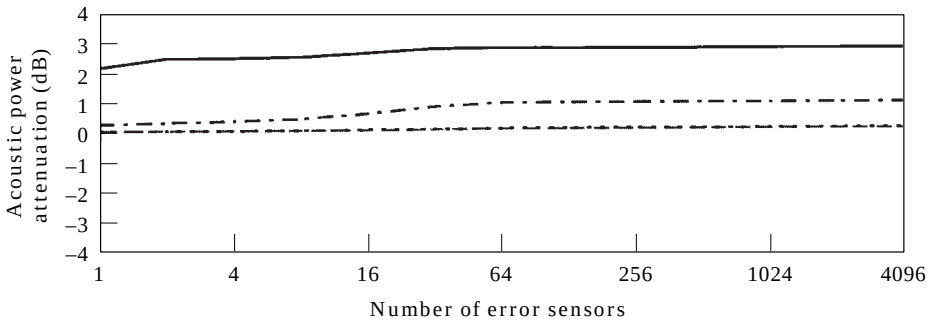

Figure 15. Sound power attenuation as a function of error sensor number for minimization of the sum of each cost function: ·– ·– ·–, potential; ------, kinetic; · · · · · · · · · , total energy; ——, intensity. The sensors are located evenly on the circle with a radius of $0{\cdot}18\lambda$ centred at the acoustic centre of the primary and control sources. Dipole-like pair of primary sources and a single monopole control source separated by $\lambda/3$.

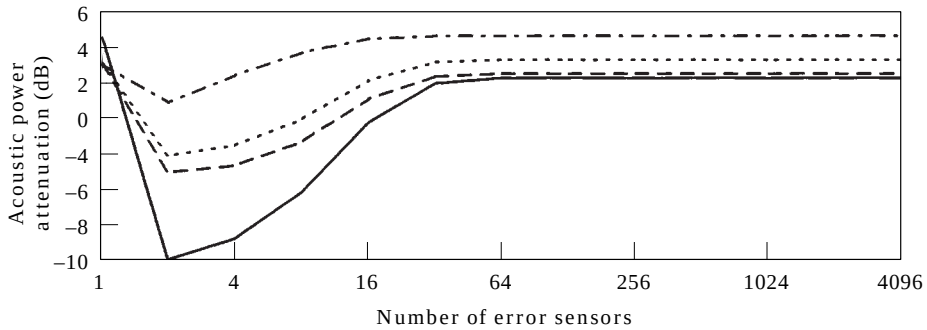

Figure 16. Sound power attenuation as a function of error sensor number for minimization of the sum of each cost function: ·– ·– ·–, potential; ------, kinetic; · · · · · · · · · , total energy; ——, intensity.The sensors are located evenly on the circle with a radius of $\lambda/4$ centred at the acoustic centre of the primary and control sources. Dipole-like pair of primary sources and a single monopole control source separated by $\lambda/3$.

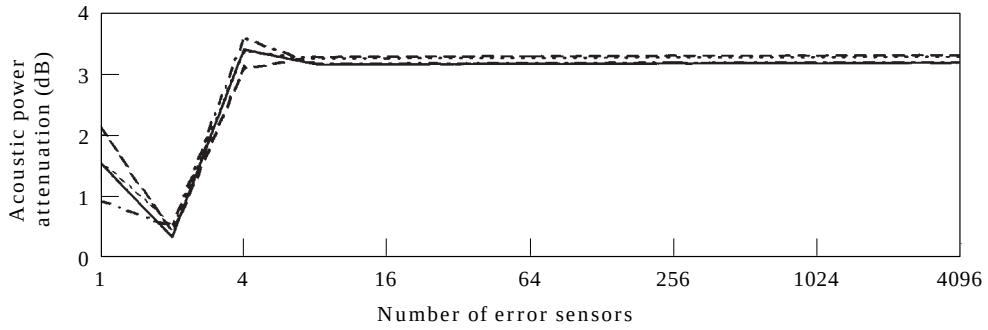

Figure 17. Sound power attenuation as a function of error sensor number for minimization of the sum of each cost function: ·– ·– ·–, potential; ------, kinetic; · · · · · · · · · , total energy; ——, intensity. The sensors are located evenly on the circle with a radius of $\lambda/2$ centred at the acoustic centre of the primary and control sources. Dipole-like pair of primary sources and a single monopole control source separated by $\lambda/3$.

source strength to minimize the sum of any criterion; when the error sensors are quite close to the sources, the acoustic power attenuation achieved by minimizing the sum of each criterion is different; the best results are obtained from minimizing the total mean active sound intensity in the radial direction.

There are also some differences for the dipole-like pair of primary sources/single monopole control source system when compared with the single monopole primary source system. The first is that more error sensors do not necessarily give better results. Sometimes introducing additional error sensors causes the acoustic power attenuation to be decreased as shown in Figures 16 and 17. The second is that at certain distances more error sensors are needed to achieve a certain acoustic power attenuation, as shown by comparing Figures 16 and 17.

It is found that minimizing the sum of the mean active intensity in the direction normal to the surface surrounding all the primary and control sources is the most effective strategy. The reason is that the total acoustic power is the objective of control and the sum of the mean active intensity in the direction normal to the surface surrounding all the primary and control sources is a good approximation of the acoustic power if a reasonable number of points are included in the sum. Because the reactive energy is relatively larger and more concentrated near the sources and there is a large mount of near field kinetic energy and

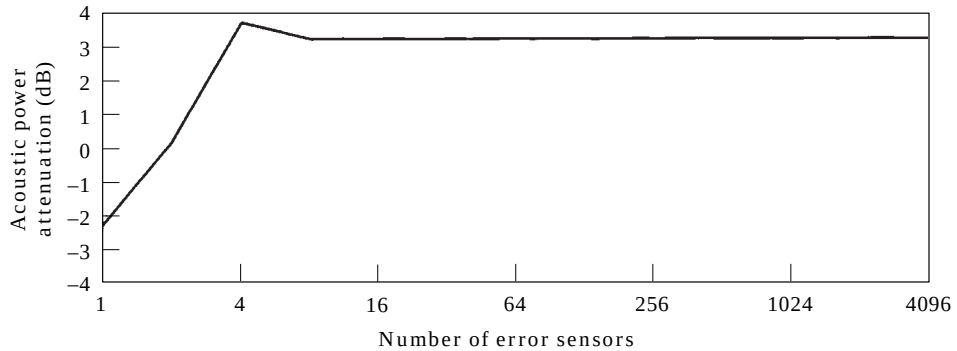

Figure 18. Sound power attenuation as a function of error sensor number for minimization of the sum of each cost function: ·– ·– ·–, potential; ------, kinetic; · · · · · · · · · , total energy; ——, intensity. The sensors are located evenly on the circle with a radius of 100λ centred at the acoustic centre of the primary and control sources. Dipole-like pair of primary sources and a single monopole control source separated by $\lambda/3$.

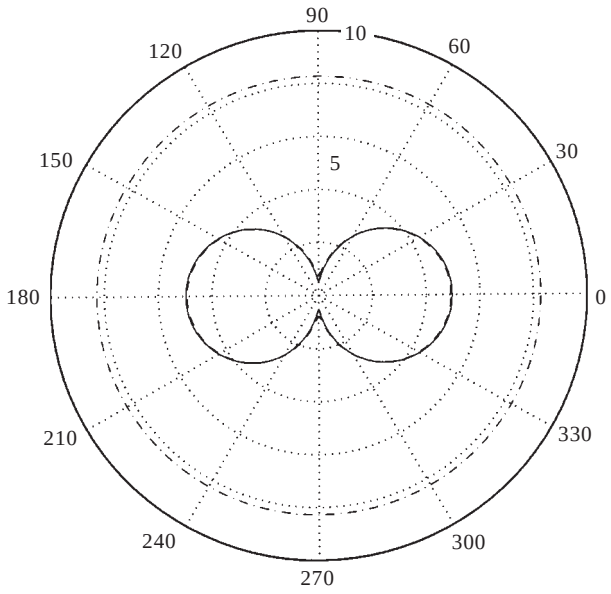

Figure 19. Angular distribution of pressure (Pa) in the far field. Single monopole primary and control sources separated by $\lambda/10$: ·–·–·–, primary source only; ------, primary plus optimum control sources (minimizing the sum of active intensities at 4096 locations in the far field); ——, primary plus optimum control sources (minimizing the total acoustic power).

potential energy that contribute little to the total acoustic power, minimizing the sum of the kinetic energy density and total energy density in the near field is not appropriate for this objective. But in the middle field (not very near field), minimizing the sum of the kinetic energy density and total energy density sometimes are the best control strategies.

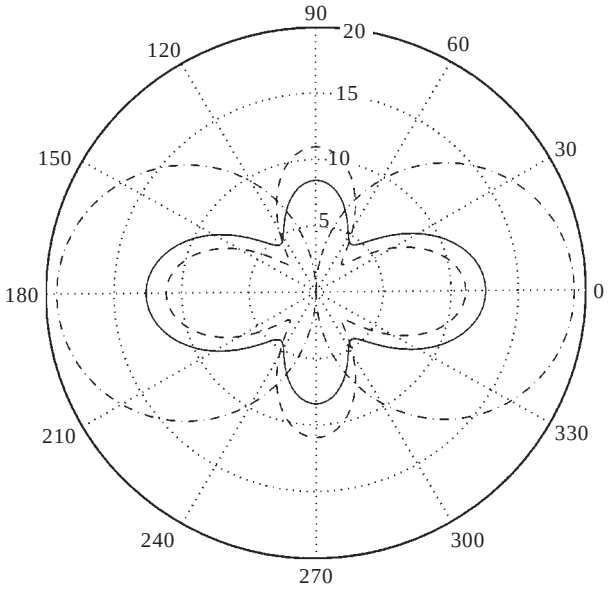

Figure 20. Angular distribution of pressure (Pa) in the far field. Dipole-like pair of primary and single monopole control sources separated by $\lambda/3$: ·–·–·–, primary source only; ------, primary plus optimum control sources (minimizing the sum of active intensities at 4096 locations in the far field); ——, primary plus optimum control sources (minimizing the total acoustic power).

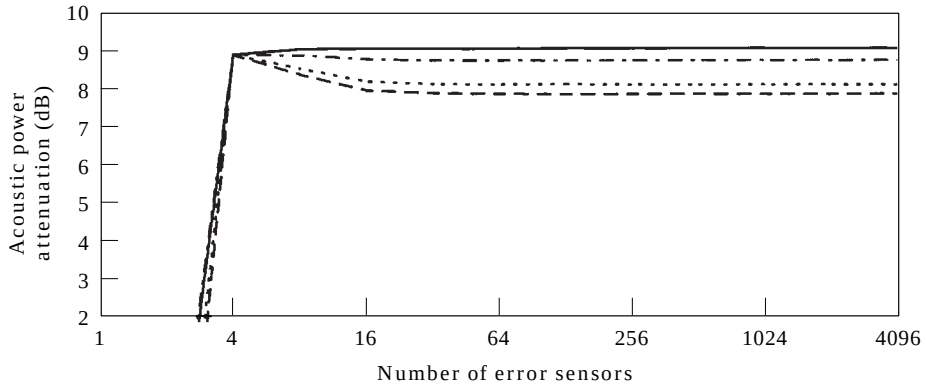

Figure 21. Sound power attenuation as a function of error sensor number for minimization of the weighted sum of each cost function: ·– ·– ·–, potential; ------, kinetic; · · · · · · · · · , total energy; ——, intensity. The sensors are located evenly on the circle with a radius of $\lambda/8$ centred at the acoustic centre of the primary and control sources. Single monopole primary and control sources separated by $\lambda/10$.

Minimizing the potential energy density in the very near field is also partly ineffective; the reason is that the use of a large number of distributed pressure sensors located near the sources may lead to an "unloading" of the whole radiation field by causing a large of area of low pressure near the sources. The overall result would be a drop in radiated power due to the low radiation impedance seen by the sources. It seems not to be the best cost function.

There is another point of note, which is that even if a very large number of error sensors are used in the far field, the system cannot reach the optimum by minimizing the sum of each cost function. As shown in Figure 18, the acoustic power attenuation produced by minimizing the sum of any cost function at 4096 locations in the far field is only 3·2 dB while the optimum is 3·7 dB. The reason can be derived from the equation below which indicates how to calculate the total radiated acoustic power by integration of the real acoustic intensity out of the sphere encompassing the sound sources.

$$W = \int_0^{2\pi} \int_0^{\pi} \mathbf{I}_r r^2 \sin\theta \, \mathrm{d}\theta \, \mathrm{d}\phi = 2\pi r^2 \int_0^{\pi} \mathbf{I}_r \sin\theta \, \mathrm{d}\theta, \tag{41}$$

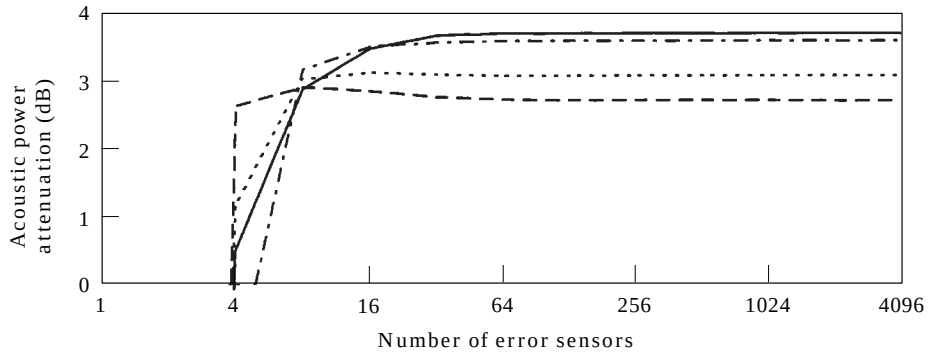

Figure 22. Sound power attenuation as a function of error sensor number for minimization of the weighted sum of each cost function: ·– ·– ·–, potential; ------, kinetic; · · · · · · · · · , total energy; ——, intensity. The sensors are located evenly on the circle with a radius of $\lambda/4$ centred at the acoustic centre of the primary and control sources. Dipole-like pair of primary sources and a single monopole control source separated by $\lambda/3$.

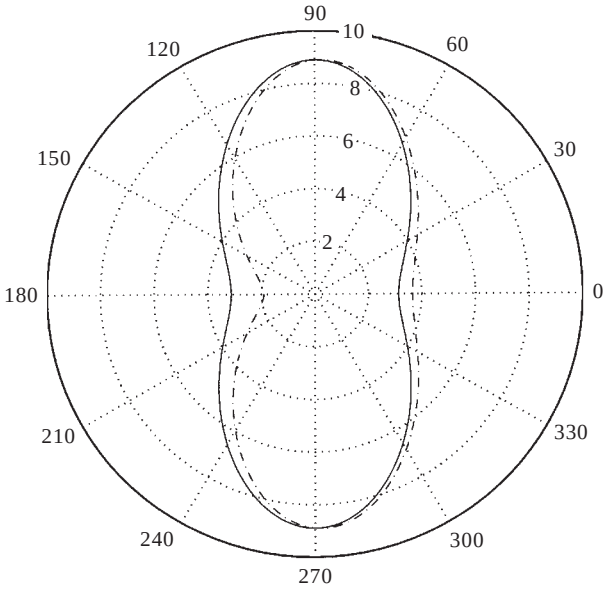

Figure 23. Maximum achievable acoustic power attenuation (dB) as a function of error sensor location along a circle surrounding the sources for the minimization of potential energy density at a point. Single monopole primary and control sources separated by $\lambda/10$: ——, far field with a radius of 100λ, –·–·– , near field with a radius of $\lambda/2$.

where r is the radius of the enclosing sphere, which is in the far field of the sources, θ is the angle between **r** and the control/primary source axis. So the best error sensor strategy is the minimization of the sum of mean active intensity in the radial direction at a number

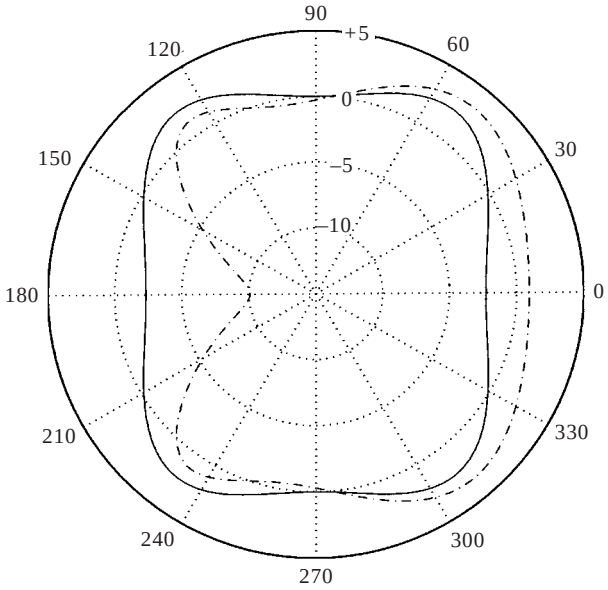

Figure 24. Maximum achievable acoustic power attenuation (dB) as a function of error sensor location along a circle surrounding the sources for the minimization of potential energy density at a point. Dipole-like pair of primary sources and single monopole control source separated by $\lambda/3$: ——, far field with a radius of 100λ; –·–·– , near field with a radius of $\lambda/2$.

of points encompassing the sound source with different weighting coefficients; the cost function is,

$$F_I = \sum_{i=1}^{N_e} \mathbf{I}(\mathbf{r}_i) \sin(\theta_i). \tag{42}$$

Figures 19 and 20 depict the distribution of pressure (units: Pa) as a function of angular location in the far field before and after active control. It is shown in Figure 19, that when minimizing the sum of the active intensities at a large number of points for the single primary and single monopole control source system, the angular distribution of total pressure is almost the same as that obtained from minimizing the total acoustic power (if the weighting coefficients are included in the cost function they will be exactly the same). However, in Figure 20, for the dipole-like pair of primary sources and single monopole control source system, it can be seen that the angular distributions of total pressure are different for minimization of the two criteria. So for more complex sound fields, the weighting coefficients must be included in the cost function.

Figures 21 and 22 show the results when the weighting coefficients $\sin\theta_i$ are included in all the cost functions as follows:

$$F_U = \sum_{i=1}^{N_e} U(\mathbf{r}_i) \sin(\theta_i), \qquad F_T = \sum_{i=1}^{N_e} T(\mathbf{r}_i) \sin(\theta_i), \qquad F_E = \sum_{i=1}^{N_e} E(\mathbf{r}_i) \sin(\theta_i), \tag{43–45}$$

$$F_I = \sum_{i=1}^{N_e} \mathbf{I}(\mathbf{r}_i) \sin(\theta_i) = \frac{1}{2} \sum_{i=1}^{N_e} \mathrm{Re}\{\mathbf{u}^*(\mathbf{r}_i) p(\mathbf{r}_i) \sin(\theta_i)\}. \tag{46}$$

It can seen from Figures 21 and 22 that if a reasonable number of points are included in the sum, then minimizing the sum of the weighted near-field mean active intensities can give the same acoustic power attenuation as that obtained from minimizing the total acoustic power for the two systems.

Comparing near-field error sensing strategies with those of far-field error sensing, it can be seen that not only placing a sound pressure error sensor in the near-field of the primary sources is a very "risky" pursuit, but placing sound pressure error sensors in the far field of the sources is also a "risky" pursuit, as shown in Figures 23 and 24. The acoustic power attenuation produced by minimizing potential energy density at $(100\lambda, 0)$ is $-2{\cdot}3$ dB (an effective increase of 2·3 dB!) in Figure 24.

In a practical system, the primary sound fields are much more complex and so it is very difficult to select the optimum error sensor locations. Minimizing the sum of the weighted potential energy density (acoustic pressure at a number of sensors) in the far field or the sum of the weighted mean active intensity in a direction normal to the surface surrounding all the primary and control sources appear to be effective strategies to avoid the increase in power output that often occurs when adjusting control sources to produce zero pressure at one location.

5. CONCLUSIONS

Eight different error sensing strategies have been evaluated for the active control of harmonic free-field sound radiated by a monopole primary source and by a dipole-like pair of primary sources. The control source was a monopole radiating at the same frequency and the criterion used to assess the error sensor strategies was the minimization of the total

radiated acoustic power. These error sensing strategies were minimization of the acoustic potential energy density, acoustic kinetic energy density, total acoustic energy density and mean active sound intensity at a point and the minimization of the sum of each of them at a number of points in the near field.

From the results obtained using the eight error sensor strategies, the following conclusions can be drawn at least for the cases studied here. First, in the far field all the eight criteria give the same results and in the near field, if one region is good for one criterion, it is usually also a good error sensor location region for the others and *vice versa*. Second, it is impossible to obtain a cost function which can always be the best, despite the distance of the error sensors from the control sources and the number of error sensors. Last, when the error sensors are quite close to the control sources, the best error sensing strategy is minimizing the sum of the mean active sound intensity in the radial direction, and close to optimal results can be achieved with a relatively small number of sensors.

An experimental implementation of the proposed method is now being undertaken for the active control of noise radiated by a large power transformer.

ACKNOWLEDGMENT

The research described in this publication was funded partly by a grant from the Electricity Supply Association of Australia Limited.

REFERENCES

1. W. B. Conover 1956 *Noise Control*, **2**, 78–82. Fighting noise with noise.
2. C. F. Ross 1978 *Journal of Sound and Vibration* **61**, 473–480. Experiments on the active control of transformer noise.
3. N. Hesselmann 1978 *Applied Acoustics* **11**, 27–34. Investigation of noise reduction on a 100 kVA transformer tank by means of active methods.
4. O. L. Angevine 1981 in *Proceedings of Internoise*'81, 303–306. Active acoustic attenuation of electric transformer noise.
5. T. Berge, O. Kr. Ø Pettersen and S. Sørsdal 1988 *Applied Acoustics*, **23**, 309–320. Active cancellation of transformer noise: field measurements.
6. O. L. Angevine 1992 in *Proceedings of Internoise*'92, 313–316. Active cancellation of the hum of large electric transformers.
7. O. L. Angevine 1995 *International Journal of Active Control* **1**, 65–78. Active systems for attenuation of noise.
8. M. McLoughlin, S. Hidebrand and Z. Hu 1994 in *Proceedings of Internoise*'94, 1323–1326. A novel active transformer quieting system.
9. G. Mangiante 1993 *Noise Control Engineering Journal* **41**, 339–345. The JMC method for 3D active sound absorption: a numerical simulation.
10. P. A. Nelson, A. R. D. Curtis, S. J. Elliott and A. J. Bullmore 1987 *Journal of Sound and Vibration* **116**, 397–414. The minimum power output of free field point source and active control of sound.
11. A. J. Kempton 1976 *Journal of Sound and Vibration* **48**, 475–483. The ambiguity of acoustic sources: a possibility for active noise control?
12. J. S. Bolton, B. K. Gardner and T. A. Beauvilain 1995 *Journal of the Acoustical Society of America* **98**, 2343–2362. Sound cancellation by the use of secondary multipoles.
13. P. A. Nelson and S. J. Elliott 1992 *Active Control of Sound*. London: Academic Press.
14. C. H. Hansen and S. D. Snyder 1997 *Active Control of Noise and Vibration*. London: E&FN Spon.
15. T. Martin and A. Roure 1997 *Journal of Sound and Vibration* **201**, 577–593. Optimisation of an active noise control system using spherical harmonic expansion of the primary field.
16. R. L. Clark and C. R. Fuller 1990 *Journal of the Acoustical Society of America* **91**, 3321–3329. Modal sensing of efficient radiators with PVDF distributed sensors in active structural acoustic control approaches.

17. J. P. Maillard and C. R. Fuller 1995 *Journal of the Acoustical Society of America* **98**, 2613–2621. Advanced time domain wave-number sensing for structural acoustic system. Part III. Experiments on the active broadband radiation control of a simply supported plate.
18. S. D. Snyder, N. Tanaka, K. A. Burgemeister and C. H. Hansen 1995 *Proceedings of Active* '95, 849–860. Institute of Noise Control Engineering. Direct-sensing of global error criteria for active noise control.
19. N. Tanaka, S. D. Snyder and C. H. Hansen 1996 *Journal of Vibration and Acoustics* **118**, 630–640. Distributed parameter modal filtering using smart sensors.
20. B. S. Cazzolato and C. H. Hansen 1998 *Journal of the Acoustical Society of America* Accepted. Active control of sound transmission using structural error sensing.
21. B. T. Wang and C. R. Fuller 1992 *Journal of the Acoustical Society of America* **92**, 1489–1498. Near-field pressure, intensity, and wave-number distributions for active structural acoustic control of plate radiation: theoretical analysis.
22. S. W. Kang and Y. H. Kim 1997 *Journal of Sound and Vibration* **201**, 595–611. Active intensity control for the reduction of radiated duct noise.
23. A. C. Zander and C. H. Hansen 1993 *Journal of the Acoustical Society of America* **94**, 841–848. A comparison of error sensor strategies for the active control of duct noise.
24. S. D. Sommerfield and P. J. Nashif 1994 *Journal of the Acoustical Society of America* **96**, 300–306. An adaptive filtered-x algorithm for energy-based active control.
25. T. Loyau and J. Pascal 1988 *Journal of the Acoustical Society of America* **84**, 1744–1750. Broadband acoustic holograpgy reconstruction from acoustic intensity measurements. I: Principle of the method.
26. S. Amini, C. Ke and P. J. Harris 1990 *Journal of Vibration and Acoustics* **112**, 257–262. Iterative solution of boundary element equations for the exterior Helmoltz problem.
27. T. Santaigo and R. J. Bernhard 1993 *Proceedings of Noise-Con* 93, 601–606. Active control of the directivity of a sound source.
28. K. A. Cunefare and G. H. Koopmann 1990 *ASME Transactions Journal of Vibration and Acoustics* **113**, 387–394. A boundary element approach to optimization of active noise control sources on three-dimensional structures.
29. K. A. Cunefare and G. H. Koopmann 1991 *Journal of the Acoustical Society of America* **90**, 365–373. Global optimum active noise control: surface and far field effects.
30. F. J. Fahy 1989 *Sound Intensity*. Amsterdam: Elsevier Science.
31. P. M. Morse and K. U. Ingard 1968 *Theoretical Acoustics*. New York: McGraw-Hill.